

This discussion paper is/has been under review for the journal Atmospheric Chemistry and Physics (ACP). Please refer to the corresponding final paper in ACP if available.

Modeling nitrous acid and its impact on ozone and hydroxyl radical during the Texas Air Quality Study 2006

B. H. Czader¹, B. Rappenglück¹, P. Percell¹, D. W. Byun^{1,2,†}, F. Ngan^{*}, and S. Kim^{**}

¹University of Houston, Department of Earth and Atmospheric Sciences, 4800 Calhoun Rd, TX 77204-5007, Houston, USA

²Resources Laboratory, NOAA, Silver Spring, MD20910, USA

^{*}present affiliation: Air Resources Laboratory, NOAA, Silver Spring, MD20910, USA

^{**}now at: Ajou University, Suwon, South Korea

[†]author deceased

Received: 14 January 2012 – Accepted: 7 February 2012 – Published: 23 February 2012

Correspondence to: B. H. Czader (bczader@uh.edu)

Published by Copernicus Publications on behalf of the European Geosciences Union.

Modeling nitrous acid and its impact

B. H. Czader et al.

Title Page

Abstract

Introduction

Conclusions

References

Tables

Figures

◀

▶

◀

▶

Back

Close

Full Screen / Esc

Printer-friendly Version

Interactive Discussion



Abstract

Nitrous acid (HONO) mixing ratios for the Houston metropolitan area were simulated with the Community Multiscale Air Quality (CMAQ) model for an episode during the Texas Air Quality Study (TexAQS) II in August/September 2006 and compared to in-situ MC/IC (mist-chamber/ion chromatograph) and long path DOAS (Differential Optical Absorption Spectroscopy) measurements at three different altitudes. Several HONO sources were accounted for in simulations, such as gas phase formation, direct emissions, nitrogen dioxide (NO_2^*) hydrolysis, photo-induced formation from excited NO_2^* and photo-induced conversion of NO_2 into HONO on surfaces covered with organic materials. Compared to the gas-phase HONO formation there was about a tenfold increase in HONO mixing ratios when additional HONO sources were taken into account, which improved the correlation between modeled and measured values. Concentrations of HONO simulated with only gas phase chemistry did not change with altitude, while measured HONO concentrations decrease with height. A trend of decreasing HONO concentration with altitude was well captured with CMAQ predicted concentrations when heterogeneous chemistry and photolytic sources of HONO were taken into account. Heterogeneous HONO production mainly accelerated morning ozone formation, albeit slightly. Also HONO formation from excited NO_2 only slightly affected HONO and ozone (O_3) concentrations. Photo-induced conversion of NO_2 into HONO on surfaces covered with organic materials turned out to be a strong source of daytime HONO. Since HONO immediately photo-dissociates during daytime its ambient mixing ratios were only marginally altered (up to 0.5 ppbv), but significant increase in the hydroxyl radical (OH) and ozone concentration was obtained. In contrast to heterogeneous HONO formation that mainly accelerated morning ozone formation, inclusion of photo-induced surface chemistry influenced ozone throughout the day.

Modeling nitrous acid and its impact

B. H. Czader et al.

Title Page

Abstract

Introduction

Conclusions

References

Tables

Figures

◀

▶

◀

▶

Back

Close

Full Screen / Esc

Printer-friendly Version

Interactive Discussion



1 Introduction

The importance of nitrous acid (HONO) in the chemistry of the atmosphere stems from its photo-dissociation that serves as a significant source of hydroxyl radical (OH) (Lammel and Cape, 1996; Alicke et al., 2002, 2003; Kleffmann et al., 2005). OH plays a crucial role in the oxidation of volatile organic compounds (VOCs) leading to the formation of ozone, in particular in urban areas with high burden of VOCs (see for instance Mao et al., 2010).

The occurrence of HONO in the lower atmosphere can be attributed to either direct emissions (Kirchstetter et al., 1996; Kurtenbach et al., 2001) or chemical formation. Among known chemical sources of HONO is the gas-phase formation from the reaction between OH and nitric oxide (NO) (Pagsberg et al., 1997) and heterogeneous formation on surfaces from nitrogen dioxide (NO₂) hydrolysis (Kleffmann et al., 1998; Finlayson-Pitts et al., 2003). Results from laboratory experiments and field campaigns suggest that HONO can also be formed in photolytic processes but the exact mechanism has not yet been identified (Kleffmann, 2005, 2007; Su et al., 2008). Zhou et al. (2002, 2003) point to the photolysis of nitrate (NO₃⁻) and nitric acid (HNO₃) as a source of HONO while the chamber study of Rohrer et al. (2005) excluded photolysis of nitrate as a HONO precursor. George et al. (2005) and Stemmler et al. (2006, 2007) observed a photo-induced conversion of NO₂ to HONO on surfaces covered with humic acid and other similar organic compounds. Several studies pointed to HONO formation initiated by the electronic excitation of NO₂; however, they differ in an explanation of the exact mechanism of this process, and correspondingly, the yield of HONO formation (Crowley and Carl, 1997; Li et al., 2008, 2009; Carr et al., 2009; Amedro et al., 2011).

A number of studies reported modeling of HONO formation from different sources and its impact on ozone concentrations. Li et al. (2010) performed 3-D model simulations with the WRF-CHEM model for Mexico City in which they accounted for several HONO sources. They concluded that addition of HONO sources other than gas-phase chemistry significantly affect HO_x (HO_x = OH + HO₂) in Mexico City leading to a midday

ACPD

12, 5851–5880, 2012

Modeling nitrous acid and its impact

B. H. Czader et al.

Title Page

Abstract

Introduction

Conclusions

References

Tables

Figures

◀

▶

◀

▶

Back

Close

Full Screen / Esc

Printer-friendly Version

Interactive Discussion



average increase in O_3 of about 6 ppb. Sarwar et al. (2008) performed CMAQ modeling of HONO for the north-eastern area of the US in which, in addition to the gas phase chemistry, HONO emissions, heterogeneous HONO formation involving NO_2 and H_2O and the photolysis of HNO_3 adsorbed on surfaces were accounted for. This approach improved surface HONO predictions and resulted in an average ozone increase of 1.4 ppbv. The recent study of Wong et al. (2011) for Houston showed that HONO production on the surface is the major source of HONO and deposition the major removal pathway. This study concentrated on nighttime HONO and was limited to a use of 1-D model that simplifies transport processes.

The Houston-Galveston-Brazoria (HGB) area has one of the highest ozone concentrations in the US often exceeding the National Ambient Air Quality Standard for ozone (Berkowitz et al., 2004; Daum et al., 2004; Wilczak et al., 2009). Since high HONO concentrations were measured in Houston during several air quality campaigns, e.g. in 2006 (Stutz et al., 2010; Ziemba et al., 2010) and thereafter repeatedly in 2009 and 2010 (unpublished), it is important to evaluate the impact of HONO on ozone for this region. The present study assesses sources and losses of HONO and its impact on ozone and HO_x formation. HONO is simulated with a three dimensional Community Multiscale Air Quality (CMAQ) model which includes HONO gas-phase chemistry, heterogeneous chemistry, and emissions, as well as two new sources that we implemented, which are formation from electronically excited NO_2 and formation from photo-induced reaction of NO_2 on surfaces covered with organic materials. Of particular interest is the analysis of different HONO sources during day and nighttimes and their impact on atmospheric chemistry. The process analysis (PA) tool that provides information on how different physical and chemical processes affect simulated concentrations was utilized for that purpose. The effects of deposition, transport and chemical reactions on HONO as well as O_3 and HO_x mixing ratios are analyzed. The simulated concentrations of HONO are compared with in-situ as well as with long-path measurements at three different altitudes obtained in Houston, Texas.

**Modeling nitrous acid
and its impact**

B. H. Czader et al.

[Title Page](#)[Abstract](#)[Introduction](#)[Conclusions](#)[References](#)[Tables](#)[Figures](#)[I◀](#)[▶I](#)[◀](#)[▶](#)[Back](#)[Close](#)[Full Screen / Esc](#)[Printer-friendly Version](#)[Interactive Discussion](#)

2 Model configuration

Simulations for this study were performed with the CMAQ model version 4.7.1, released by the US Environmental Protection Agency (EPA) (Byun and Schere, 2006). For the purpose of deriving reliable boundary conditions CMAQ was run with 36 km grid resolution for the domain covering Continental US, North Mexico, and South Canada and with 12 km grid resolution for the Texas domain. Current analysis is based on the simulations performed with 4 km grid resolution for the domain covering the HGB area. The atmosphere was divided into 23 vertical layers between the surface and 50 mbar (around 20 km height). Chemical reactions were simulated with the SAPRC-99 chemical mechanism (Carter, 1990, 2000) that included aerosol and aqua chemistry (saprc99_ae5_aq). Integrated process rate (IPR) analysis was carried out to track contributions of chemical and transport processes to HONO mixing ratios. In addition, integrated reaction rate (IRR) analysis was employed to investigate chemical sources and losses for HONO as well as its impact on radical and ozone formation. Simulations were performed for the 25 August–21 September, 2006 time period that coincides with the Texas Air Quality Study II. Two days spin-up time was used to obtain realistic initial conditions.

Meteorological data were simulated with the Mesoscale Model, version 5 (MM5) (Grell et al., 1994). An updated land use and land cover data as described in Cheng and Byun (2008) was utilized in those simulations. To further improve meteorological variables a multi-nest grid-nudging based on Four-Dimensional Data Assimilation (FDDA) with the Texas CAMS and NOAA Meteorological Assimilation Data Ingest System (MADIS) was performed (Ngan et al., 2011). Conversion of the meteorological data to CMAQ inputs was performed with the Meteorological Chemistry Interface Processor (MCIP) (Byun and Schere, 2006).

Gridded emissions were derived with the Sparse Matrix Operator Kernel Emissions (SMOKE) system (Houyoux et al., 2000) using the Texas inventory, including hourly-specific Texas Point-source Special Inventory (TPSI2006) for the year 2006,

Modeling nitrous acid and its impact

B. H. Czader et al.

Title Page

Abstract

Introduction

Conclusions

References

Tables

Figures

◀

▶

◀

▶

Back

Close

Full Screen / Esc

Printer-friendly Version

Interactive Discussion



the Base5b 2007 area and non-road emissions, 2006 biogenic emissions, and mobile emissions derived from “linked based” and the High Performance Monitoring System (HPMS) data (available at: ftp://ftp.tceq.state.tx.us/pub/OEPAA/TAD/Modeling/HGB8H2/ei06). For SMOKE processing the Texas emission inventory was converted from the AIRS Facility Subsystem (AFS) to the Inventory Data Analyzer (IDA) format. Locations of point sources in the Lambert Conformal Conic (LCC) map projection format were converted into latitude-longitude (LL) coordinates for spatial allocation in SMOKE. The National Emission Inventory v. 2002 (NEI2002) was utilized for areas not covered by the Texas inventory.

2.1 HONO sources

In addition to the gas-phase HONO chemistry, the CMAQ version used in this study accounts for the heterogeneous formation of HONO on urban, leaves, and particle surfaces (Foley et al., 2009) with a reaction rate coefficient $k = 5 \times 10^{-5} \times (S/V) [s^{-1}]$ as measured by Kurtenbach et al. (2001), where S/V is the ratio of a surface area to volume of air. For this study we implemented two additional photo-dependent HONO sources into CMAQ as described below.

Stemmler et al. (2006, 2007) showed that HONO can be formed from the photo-induced reaction of NO_2 on surfaces covered with humic acid and similar organic materials. George et al. (2005) also observed photo-enhanced HONO production on solid organic compounds. These studies suggested that the uptake coefficient for reaction with organics is much larger than the one for heterogeneous reaction and that it depends on solar radiation. Enhanced photochemical production of HONO was also reported by Ndour et al. (2008) and Monge et al. (2010). Based on these studies Li et al. (2010) implemented a daytime HONO source with an uptake coefficient of 2×10^{-5} for light intensities less than $400 W m^{-2}$ and an uptake coefficient scaled by (light intensity)/400 for solar radiation larger than $400 W m^{-2}$. We adopted this approach for CMAQ simulations for Houston, but obtained unrealistically high HONO concentrations. Therefore, contrary to Li et al. (2010) our approach do not employ a threshold value

Modeling nitrous acid and its impact

B. H. Czader et al.

Title Page

Abstract

Introduction

Conclusions

References

Tables

Figures

◀

▶

◀

▶

Back

Close

Full Screen / Esc

Printer-friendly Version

Interactive Discussion



for solar radiation as we used an uptake coefficient of 2×10^{-5} scaled by (light intensity)/900, where light intensity at local noon reaches about 900 W m^{-2} . According to the following equation for the reaction rate coefficient:

$$k = \frac{1}{8} v_{\text{NO}_2} \left(\frac{S}{V} \right) r_g \quad (1)$$

5 where v_{NO_2} is the mean molecular speed of NO_2 , S/V is the surface to volume ratio, and r_g is the reactive uptake coefficient, the reaction uptake coefficient r_g of 2×10^{-5} resulted in a reaction rate coefficient k of $1 \times 10^{-3} \times (S/V) [\text{s}^{-1}]$ scaled to (light intensity/900).

Formation of HONO initiated by excitation of NO_2 was confirmed by several studies. Li et al. (2008) reported that the excited NO_2 (indicated as NO_2^*) reacts with water to produce HONO and determined a reaction rate coefficient of $1.7 \times 10^{-13} \text{ cm}^3 \text{ s}^{-1}$. Carr et al. (2009) and Amedro et al. (2011) suggested that this is a two step process involving two NO_2^* molecules, and consequently, less efficient than the one reported by Li et al. (2008). In our study we adopted Li et al. (2008) approach; therefore, our results provide an upper bound of the impact of this reaction on atmospheric chemistry. The excess energy of excited NO_2 can also be released upon collision with nitrogen, oxygen, or water; therefore, these reactions were also accounted for in the model. The impact of this reaction was subject of several studies. While the modeling study of Wennberg and Dabdub (2008) show that excited NO_2 chemistry causes significant ozone increase in California (up to 55 ppb) when modeled for past period (1987) when still high NO_x emissions were observed, Ensberg et al. (2010) obtained much smaller impact on ozone when lower NO_x emissions occurring in 2005 were simulated.

HONO emissions from mobile sources, non-road sources, such as construction and lawn equipment, as well as off-road sources, such as emissions from ships, locomotives, and aircraft were estimated based on the Kurtenbach et al. (2001) formula $\text{HONO}/\text{NO}_x = 8 \times 10^{-3}$.

Modeling nitrous acid and its impact

B. H. Czader et al.

Title Page

Abstract

Introduction

Conclusions

References

Tables

Figures

◀

▶

◀

▶

Back

Close

Full Screen / Esc

Printer-friendly Version

Interactive Discussion



Three simulations were performed using different HONO sources and are indicated as follow:

1. G – **g**as-phase HONO chemistry;
2. GEH – **g**as phase chemistry, HONO **e**missions, and HONO **h**eterogeneous formation;
3. GEHP – same as GEH, but with addition of **p**hoto-induced HONO production.

3 Results and discussion

3.1 Evaluation of HONO modeling

Simulated HONO concentrations were compared with values measured in-situ by a mist-chamber/ion chromatograph (MC/IC) system at the top of the Moody Tower on the University of Houston (UH) campus (Stutz et al., 2010) as shown in Fig. 1 for simulation cases G, GEH, and GEHP. The highest HONO mixing ratios up to 2 ppbv were measured during nighttimes and in the early mornings while daytime concentrations are much lower, but still appreciable. HONO values simulated with only gas-phase chemistry (case G) persistently show significant under prediction of HONO concentrations. HONO mixing ratios from GEH and GEHP cases are much closer to the observed values (e.g. 31 August, 12 and 20 September). In some cases a mismatch between observed and simulated HONO values occurs (e.g. 1 and 6 September). This is mostly related to mismatch in NO₂ concentrations as discussed further below. Figure 2 shows an average diurnal variation of HONO and NO₂ based on the same data set (25 August–21 September 2006) for observed and simulated cases. It can be seen that higher daytime values were obtained from the GEHP case, which includes photolytic HONO formation. Nighttime and morning overprediction of HONO can be attributed to NO₂ overprediction.

Modeling nitrous acid and its impact

B. H. Czader et al.

Title Page

Abstract

Introduction

Conclusions

References

Tables

Figures

◀

▶

◀

▶

Back

Close

Full Screen / Esc

Printer-friendly Version

Interactive Discussion



In order to evaluate HONO modeling for different altitudes in the urban boundary layer observational HONO data detected by Differential Optical Absorption Spectroscopy (DOAS) were utilized. These measurements were taken along different paths between the Moody Tower super site and Downtown Houston (Stutz et al., 2010). The low light-path detected mixing ratios between 20–70 m height which corresponds to the first and second CMAQ model layer, the middle light-path between 70–130 m corresponding to the second and third layer, and the upper light-path between 130–300 m, which falls into model layers three to five. Figure 3 shows a comparison of measured and simulated HONO values. While daytime measurements do not show dependence with altitude, HONO mixing ratios at night and early morning decrease with altitude, with maxima reaching about 2 ppbv at the low level and 0.5 ppbv at the upper level. Contrary to the measured values, HONO mixing ratios from the G case do not show variation with height while HONO values obtained from GEH and GEHP cases correctly capture the trend towards lower nighttime and early morning mixing ratios at higher altitudes. Addition of photolytic HONO sources in the GEHP case resulted in average 100 ppt higher daytime HONO concentrations at the low DOAS level as compared to the GEH case and an average daytime increase of 50 and 30 ppt at the middle and upper DOAS levels, respectively. Since most of the photolytic HONO production occurs by NO_2 reaction at the surface, changes in HONO mixing ratios at higher altitudes can be explained by upward transport of HONO (see discussion in Sect. 3.2 and bottom graph in Fig. 9).

There are cases when simulated HONO time series do not match the measured data. For example, HONO is over predicted by the model on 1 and 4 September, and under predicted during the night of 5–6 September and morning of 7 and 8 September. Since NO_2 is a direct precursor of HONO, a mismatch between modeled and simulated HONO can be linked to the mismatch of NO_2 . Figure 4 shows a time series comparison of measured NO_2 with the values simulated with the GEH case. Too high NO_2 concentrations on 1 and 4 September resulted in over prediction of HONO concentrations at those times. In contrast, NO_2 under prediction on 2, 7, and 8 September leads to

**Modeling nitrous acid
and its impact**

B. H. Czader et al.

Title Page

Abstract

Introduction

Conclusions

References

Tables

Figures

◀

▶

◀

▶

Back

Close

Full Screen / Esc

Printer-friendly Version

Interactive Discussion



under predictions of HONO. There may be several reasons for NO_2 mismatches, such as uncertainties in emission inventory or mixing layer height, in some cases these mismatches can be related to predictions of meteorological parameters. For example, on the night of 1 September the measurements indicate calm conditions, while the model predicts strong southerly winds, causing lower modeled concentrations at the location of measurements. On 6 September the model fails to predict precipitation correctly which in turn directly affects the concentration of pollutants. The correlation coefficient between HONO values measured at the low path and those simulated with GEH case is 0.68. However, when data points with wrong NO_2 prediction were ignored and only NO_2 values simulated within 70 % of measured value were considered the correlation coefficient for HONO increased to 0.82.

3.2 Impact of HONO on HO_x and ozone formation

The top graph in Fig. 5 shows a comparison of observed and modeled OH radical for 31 August 2006. OH was measured with the Ground-based Tropospheric Hydrogen Oxides Sensor (GTHOS) from the top of the Moody Tower (Mao et al., 2010). Modeled concentration of OH from the GEH case is similar to the G case, while there is twice as much OH from the GEHP case as compared to GEH case during morning hours and about 7 % more OH around noon. To assess OH sources the IRR analysis was employed in which data were averaged in a box consisting of 25 horizontal cells with the middle cell corresponding to the location of the Moody Tower. The bottom graph in Fig. 5 shows IRR results for the sum of reactions $\text{HONO} + h\nu \rightarrow \text{OH} + \text{NO}$ and $\text{NO}_2^* + \text{H}_2\text{O} \rightarrow \text{OH} + \text{HONO}$ that can be interpreted as the amount of OH produced from these two reactions. To assess the impact of NO_2^* on OH formation additional simulation was performed in which photochemical HONO formation on surfaces covered with organic materials was not included, this simulation is indicated in the graph as “GEHP (no surf phot)”. During morning hours OH production from the GEHP case was 2–3 times higher than production from the case without photochemical HONO formation (the GEH case). Reactions involving NO_2^* contributed only about 30 % to that

Modeling nitrous acid and its impact

B. H. Czader et al.

[Title Page](#)[Abstract](#)[Introduction](#)[Conclusions](#)[References](#)[Tables](#)[Figures](#)[◀](#)[▶](#)[◀](#)[▶](#)[Back](#)[Close](#)[Full Screen / Esc](#)[Printer-friendly Version](#)[Interactive Discussion](#)

increase. The additional OH reacted leading to additional O₃ formation in GEHP case (see Figs. 7 and 8) but also is reflected in higher OH mixing ratios.

IRR analysis was also employed to assess HONO contribution to radical production relative to other radical sources. Due to the fast chemistry between OH and the hydroperoxyl radical (HO₂) both radicals were considered in the analysis as HO_x (HO_x = OH + HO₂). Since the simulated HONO values for 31 August are well correlated with measured data (see Figs. 1 and 3), the HO_x analysis is performed for that day. Figure 6 illustrates the diurnal variations of contributions of O₃, HCHO, HONO (from photolysis reaction), NO₂^{*}, and alkenes to the HO_x budget. The results from the G case show that the contribution of HONO to the HO_x formation rates in the morning (06:00–09:00 a.m. CST) is 45 %, which is low in comparison to other studies. For example, Mao et al. (2010) demonstrated that in the Houston area HONO is the major contributor to HO_x in the morning. In our model analysis the morning contribution of HONO to HO_x formation rates in Houston became dominant (81 %) when HONO emissions and heterogeneous chemistry is taken into account (GEH case). In the GEHP case HONO contributes 83 % to HO_x formation and NO₂^{*} contributes 7 % by directly forming OH radical. The GEHP case also resulted in higher contributions throughout the day, especially between 09:00 a.m. and noon CST when HONO contribution to HO_x is 52 % (20 % higher than contribution from GEH case at that time).

Figure 7 shows comparison of observed and simulated ozone concentrations at the three DOAS levels for simulated time period of 25 August–21 September 2006. As it is hard to distinguish differences in ozone concentration among the simulated cases the insert in Fig. 7 shows details for the DOAS low path level on 31 August 2006. Compared to simulations with gas phase HONO chemistry ozone concentration in the GEH case only slightly increases in the morning, but increases by about 7 ppbv and accelerates morning ozone formation for about 1–2 h when photo-induced HONO production is accounted for in the GEHP case. Figure 8 shows spatial differences in ozone between the GEH and G cases (left) and for the GEHP and G case (right) for 31 August 2006, at 09:00 a.m. CST (top) and 01:00 p.m. CST (bottom). Ozone increase from the GEH

**Modeling nitrous acid
and its impact**

B. H. Czader et al.

Title Page

Abstract

Introduction

Conclusions

References

Tables

Figures

◀

▶

◀

▶

Back

Close

Full Screen / Esc

Printer-friendly Version

Interactive Discussion



case reached 3 ppbv at 09:00 a.m. CST on 31 August 2006, a day with very high HONO concentrations, while at the same time ozone differences for the GEHP case are around 8 ppbv. In the afternoon ozone changes in the GEH case reach only 2 ppbv and are confined to a smaller area, while in the GEHP case ozone increased up to 11 ppbv in comparison to the G case.

Even though about a tenfold increase in HONO concentration related to its heterogeneous formation and emissions was simulated with the GEH case (see Figs. 1 and 3) as compared to the G case, the impact of it on ozone was small. To get more insights into sources and losses of HONO the process analysis (PA) was utilized. The results of the process analysis for the G, GEH, and GEHP cases are presented in Fig. 9. Processes that contribute to an increase in HONO mixing ratios are plotted with positive values, and those contributing to a decrease in HONO mixing ratio are shown with negative values. Note that the rate of change at a given hour represents change in HONO mixing ratio between that hour and the previous hour. Since most of the HONO sources occur on the surface this analysis is confined to the first model layer (0–34 m a.g.l.); horizontally data was averaged in 25 cells with the middle cell corresponding to the location of the Moody Tower. In the G case, the gas-phase chemistry (GAS_PROD_HONO) contributes the most to an increase in HONO mixing ratio; about 60 % of produced HONO is consumed by means of photolysis and reaction with OH during daytime (indicated in the graph as CHEM_LOSS_HONO), about 20 % is deposited to the ground, and 20 % removed by transport processes. In the GEH case, 71 % of HONO production is caused by heterogeneous surface chemistry (HET_HONO) during nighttime and early morning. The accumulation of HONO formed by heterogeneous chemistry and emitted during nighttime leads to the peak HONO concentration that occurs around 06:00 a.m. CST (which is 3–4 h earlier in comparison to the G case). At that time direct HONO emissions contribute 27 %. During daytime contribution from emissions increases to 50 %, while heterogeneous and gas formation contributes 31 % and 19 %, respectively. The main removal of HONO from the surface layer is through upward transport (VTRAN_HONO) that contributes 77 % to nighttime

**Modeling nitrous acid
and its impact**

B. H. Czader et al.

[Title Page](#)[Abstract](#)[Introduction](#)[Conclusions](#)[References](#)[Tables](#)[Figures](#)[◀](#)[▶](#)[◀](#)[▶](#)[Back](#)[Close](#)[Full Screen / Esc](#)[Printer-friendly Version](#)[Interactive Discussion](#)

and 65 % to daytime reduction in HONO concentration. Dry deposition removes 23 % and 12 % of HONO during nighttime and daytime, respectively. 24 % of daytime HONO reacts to form OH. Although dry deposition and vertical transport are significant HONO removal processes during nighttime, the production of HONO is higher leading to a net increase of HONO concentration that result in the morning peak. After sunrise photochemical reactions add to the removal of HONO resulting in a decrease of HONO concentration. There are two additional pathways of photochemical HONO production in the GEHP case, these are photochemical formation on surfaces covered with organic material (hv_SF_HONO) and formation from excited NO_2 ($hv_NO_2^*_HONO$). Although we used the largest reaction coefficient for HONO formation from excited NO_2 it resulted in small amount of HONO produced by this pathway, which is even less than that from gas phase chemistry, being negligible compared with other HONO production mechanisms. The photochemical formation on the surfaces has a major contribution of 61 % to HONO production during daytime. This production is overtaken mainly by vertical transport and chemical reactions leading to a net decrease in daytime HONO mixing ratios. HONO chemical loss ($CHEM_LOSS_HONO$) immediately after sunrise is more significant in the GEHP case than the GEH case. About twice as much HONO photo-dissociates in the GEHP case producing twice as much OH and NO as compared to the GEH case. As previously shown, this additional OH resulted in higher OH and O_3 mixing ratios in the GEHP case (see Figs. 5, 7, and 8).

4 Conclusions

CMAQ simulations of HONO that included several sources of HONO were performed and compared with MC/IC measured values at the Moody Tower and DOAS measurements at three altitudes. In addition, source and losses for HONO as well as the impact of its different sources on HO_x and O_3 were examined. Accounting for additional HONO production (e.g. heterogeneous HONO formation) as compared to gas-phase formation resulted in about a tenfold increase in the morning HONO concentrations causing

Modeling nitrous acid and its impact

B. H. Czader et al.

Title Page

Abstract

Introduction

Conclusions

References

Tables

Figures

◀

▶

◀

▶

Back

Close

Full Screen / Esc

Printer-friendly Version

Interactive Discussion



improved correlation between modeled and measured values. Also, for the first time a 3-D chemistry transport model such as CMAQ could be successfully validated against vertically resolved HONO measurements during day and nighttime, and was able to capture correctly a trend of decreasing HONO concentration with altitude. Since NO_2 is a precursor of HONO the mismatches in NO_2 modeling directly influence HONO predictions.

Heterogeneous HONO production is a major source of HONO during nighttime leading to HONO accumulation and early morning peak concentration of up to 2 ppbv. Since HONO dissociation at that time is less important than deposition and vertical transport, heterogeneous HONO production only slightly increases concentrations of OH and O_3 (up to 3 ppbv ozone increase). The implementation of additional photo-dependent HONO sources, in particular HONO formation from the photo-induced reaction of NO_2 on surfaces covered with humic acid and similar organic materials, only resulted in an increase in HONO mixing ratios of at most 0.5 ppbv. However, process analysis shows that actually much more HONO was produced but quickly dissociated, which resulted in doubled morning production of hydroxyl radical and an ozone increase of up to 11 ppbv. In contrast to heterogeneous HONO formation that mainly accelerates morning ozone formation, inclusion of HONO photochemical sources influences ozone throughout the day, affecting its peak concentration.

Although daytime HONO formation mechanisms may not be understood in all details and the implementation of it to the model is based on many assumptions and simplifications, for example the estimation of reactive surfaces or uncertainties in the uptake coefficient, this paper demonstrates that photochemical HONO formation can be a strong source of daytime HONO that directly impacts OH mixing ratios and peak ozone concentrations while nighttime and early morning HONO production by means of NO_2 hydrolysis greatly affects the HONO morning peak concentration but only slightly increases hydroxyl radical and ozone concentrations.

**Modeling nitrous acid
and its impact**

B. H. Czader et al.

Title Page

Abstract

Introduction

Conclusions

References

Tables

Figures

I◀

▶I

◀

▶

Back

Close

Full Screen / Esc

Printer-friendly Version

Interactive Discussion



Acknowledgements. The authors would like to thank the Houston Advanced Research Center (HARC) for support. Observational DOAS data provided by Jochen Stutz, UCLA and MC/IC data provided by Jack Dibb, UNH. OH data provided by Bill Brune, Penn State University.

References

- 5 Aliche, B., Platt, U., and Stutz, J.: Impact of nitrous acid photolysis on the total hydroxyl radical budget during the limitation of oxidant production/Pianura Padana Produzione di Ozono study I Milan, *J. Geophys. Res.*, 107, 8196, doi:10.1029/2000JD000075, 2002.
- Aliche, B., Geyer, A., Hofzumahaus, A., Holland, F., Konrad, S., Pätz, H. W., Schäfer, J., Stutz, J., Volz-Thomas, A., and Platt, U.: OH formation by HONO photolysis during the BERLIOZ
10 experiment, *J. Geophys. Res.*, 108, 8247, doi:10.1029/2001JD000579, 2003.
- Amedro, D., Parker, A. E., Schoemaeker, C., and Fittschen, C.: Direct observation of OH radicals after 565 nm multi-photon excitation of NO₂ in the presence of H₂O, *Chem. Phys. Lett.*, 513, 12–16, doi:10.1016/j.cplett.2011.07.062, 2011.
- Berkowitz, C. M., Jobson, T., Jiang, G., Spicer, C. W., and Doskey, P. V.: Chemical and meteorological characteristic associated with rapid increases of O₃ in Houston, Texas, *J. Geophys. Res.*, 109, D10307, doi:10.1029/2003JD004141, 2004.
- Byun, D. and Schere, K. L.: Review of the Governing Equations, Computational Algorithms, and Other Components of the Models-3 Community Multiscale Air Quality (CMAQ) Modeling System, *Appl. Mech. Rev.*, 59, 51–77, 2006.
- 20 Carr, S., Heard, D. E., and Blitz, M. A.: Comment on “Atmospheric Hydroxyl Radical Production from Electronically Excited NO₂ and H₂O”, *Science*, 324, 336, 2009.
- Carter, W. P. L.: A Detailed Mechanism for the Gas-Phase Atmospheric Reactions of Organic Compounds, *Atmos. Environ.*, 24, 481–518, 1990.
- Carter, W. P. L.: Documentation of the SAPRC-99 chemical mechanism for VOC reactivity
25 assessment, Final Report to the California Air Resources Board, Contracts 92-32 and 95-308, Riverside, CA, available at: <http://pah.cert.ucr.edu/~simcarter/bycarter.htm>, 2000.
- Cheng, F.-Y. and Byun, D. W.: Application of high resolution land use and land cover data for atmospheric modeling in the Houston-Galveston metropolitan area – Part 1: Meteorological simulation results, *Atmos. Environ.*, 42, 7795–7811, 2008.

Modeling nitrous acid and its impact

B. H. Czader et al.

Title Page

Abstract

Introduction

Conclusions

References

Tables

Figures

◀

▶

◀

▶

Back

Close

Full Screen / Esc

Printer-friendly Version

Interactive Discussion



Crowley, J. N. and Carl, S. A.: OH Formation in the Photoexcitation of NO₂ beyond the Dissociation Threshold in the Presence of Water Vapor, *J. Phys. Chem. A*, 101, 4178–4184, 1997.

5 Daum, P. H., Kleinman, L. I., Springston, S. R., Nunnermacker, L. J., Lee, Y.-N., Weinstein-Lloyd, J., Zheng, J., and Berkowitz, C. M.: A comparative study of O₃ formation in the Houston urban and industrial plumes during the 2000 Texas Air Quality Study, *J. Geophys. Res.*, 108, 4715, doi:10.1029/2003JD003552, 2003.

10 Ensberg, J. J., Carreras-Sospedra, M., and Dabdub, D.: Impacts of electronically photo-excited NO₂ on air pollution in the South Coast Air Basin of California, *Atmos. Chem. Phys.*, 10, 1171–1181, doi:10.5194/acp-10-1171-2010, 2010.

Finlayson-Pitts, B. J., Wingen, L. M., Sumner, A. L., Syomin, D., and Ramazan, K. A.: The heterogeneous hydrolysis of NO₂ in laboratory systems and in outdoor and indoor atmospheres: and integrated mechanism, *Phys. Chem. Chem. Phys.*, 5, 223–242, 2003.

15 Foley, K. M., Roselle, S. J., Appel, K. W., Bhawe, P. V., Pleim, J. E., Otte, T. L., Mathur, R., Sarwar, G., Young, J. O., Gilliam, R. C., Nolte, C. G., Kelly, J. T., Gilliland, A. B., and Bash, J. O.: Incremental testing of the Community Multiscale Air Quality (CMAQ) modeling system version 4.7, *Geosci. Model Dev.*, 3, 205–226, doi:10.5194/gmd-3-205-2010, 2010.

20 George, C., Sterkowski, R. S., Kleffmann, J., Stemmler, K., and Ammann, M.: Photoenhanced uptake of gaseous NO₂ on solid organic compounds: a photochemical source of HONO?, *Faraday Discuss.*, 130, 195–210, 2005.

Grell, G. A., Dudhia, J., and Stauffer, D. R.: A description of the Fifth-Generation Penn State/NCAR Mesoscale Model (MM5), NCAR Technical Note, NCAR/TN-398+STR, 122 pp., available at: <http://www.mmm.ucar.edu/mm5/>, 1994.

25 Houyoux, M., Vukovich, J., and Brandmeyer, J.: Sparse Matrix Kernel Emissions Modeling System: SMOKE User Manual, MCNC-North Carolina Supercomputing Center, available at: <http://www.cmascenter.org/>, 2000.

Kirchstetter, T. W., Harley, R. A., and Littlejohn, D.: Measurements of nitrous acid in motor vehicle exhaust, *Environ. Sci. Technol.*, 30, 2843–2849, 1996.

30 Kleffmann, J.: Daytime Sources of Nitrous Acid (HONO) in the Atmospheric Boundary Layer, *Chem. Phys. Chem.*, 8, 1137–1144, doi:10.1002/cphc.200700016, 2007.

Kleffmann, J., Gavriloaiei, T., Hofzumahaus, A., Holland, F., Koppmann, R., Rupp, L., Schlosser, E., Siese, M., and Wahner, A.: Daytime formation of nitrous acid: A major source of OH radicals in a forest, *Geophys. Res. Lett.*, 32, L05818, doi:10.1029/2005GL022524,

**Modeling nitrous acid
and its impact**

B. H. Czader et al.

Title Page

Abstract

Introduction

Conclusions

References

Tables

Figures

◀

▶

◀

▶

Back

Close

Full Screen / Esc

Printer-friendly Version

Interactive Discussion



2005.

- Kleffmann, J., Becker, K. H., and Wiesen, P.: Heterogeneous NO₂ conversion processes on acid surfaces: possible atmospheric implications, *Atmos. Environ.*, 32, 2721–2729, 1998.
- Kurtenbach, R., Becker, K. H., Gomes, J. A. G., Kleffmann, J., Lörzer, J. C., Spittler, M., Wiesen, P., Ackermann, R., Geyer, A., and Platt, U.: Investigations of emissions and heterogeneous formation of HONO in a road traffic tunnel, *Atmos. Environ.*, 35, 3385–3394, 2001.
- Lammel, G. and Cape, J. N.: Nitrous acid and nitrate in the atmosphere, *Chem. Soc. Rev.*, 25, 361–39, 1996.
- Li, G., Lei, W., Zavala, M., Volkamer, R., Dusanter, S., Stevens, P., and Molina, L. T.: Impacts of HONO sources on the photochemistry in Mexico City during the MCMA-2006/MILAGO Campaign, *Atmos. Chem. Phys.*, 10, 6551–6567, doi:10.5194/acp-10-6551-2010, 2010.
- Li, S., Matthews, J., and Sinha, A.: Atmospheric Hydroxyl Radical Production from Electronically Excited NO₂ and H₂O, *Science*, 319, 1657–1660, 2008.
- Li, S., Matthews, J., and Sinha, A.: Response to Comment on “Atmospheric Hydroxyl Radical Production from Electronically Excited NO₂ and H₂O”, *Science*, 324, 336, doi:10.1126/science.1166877, 2009.
- Mao, J., Ren, X., Chen, S., Brune, W. H., Chen, Z., Martinez, M., Harder, H., Lefer, B., Rappenglück, B., Flynn, J., and Leuchner, M.: Atmospheric Oxidation Capacity in the Summer of Houston 2006: Comparison with Summer Measurements in Other Metropolitan Studies, *Atmos. Environ.*, 44, 4107–4115, doi:10.1016/j.atmosenv.2009.01.013, 2010.
- Monge, M. E., D’Anna, B., Mazri, L., Giroir-Fendler, A., Ammann, M., Donaldson, D. J., and George, C.: Light changes the atmospheric reactivity of soot, *P. Natl. Acad. Sci.*, 107, 6605–6609, 2010.
- Ndour, M., D’Anna, B., George, C., Ka, O., Balkanski, Y., Kleffmann, J., Stemmler, K., and Ammann, M.: Photoenhanced uptake of NO₂ on mineral dust: Laboratory experiments and model simulations, *Geophys. Res. Lett.*, 35, L05812, doi:10.1029/2007GL032006, 2008.
- Ngan, F., Byun, D. W., Kim, H. C., Rappenglueck, B., and Pour-Biazar, A.: Performance Assessment of Retrospective Meteorological Inputs for Use in Air Quality Modeling during TexAQ5 2006, *Atmos. Environ.*, doi:10.1016/j.atmosenv.2012.01.035, in press, 2012.
- Pagsberg, P., Bjergbakke, E., Ratajczak, E., and Sillesen, A.: Kinetics of the gas phase reaction OH + NO(+M) → HONO(+M) and the determination of the UV absorption cross section of HONO, *Chem. Phys. Lett.*, 272, 383–390, 1997.
- Rohrer, F., Bohn, B., Brauers, T., Brüning, D., Johnen, F.-J., Wahner, A., and Kleffmann,

Modeling nitrous acid and its impact

B. H. Czader et al.

Title Page

Abstract

Introduction

Conclusions

References

Tables

Figures

◀

▶

◀

▶

Back

Close

Full Screen / Esc

Printer-friendly Version

Interactive Discussion



**Modeling nitrous acid
and its impact**

B. H. Czader et al.

[Title Page](#)[Abstract](#)[Introduction](#)[Conclusions](#)[References](#)[Tables](#)[Figures](#)[◀](#)[▶](#)[◀](#)[▶](#)[Back](#)[Close](#)[Full Screen / Esc](#)[Printer-friendly Version](#)[Interactive Discussion](#)

J.: Characterisation of the photolytic HONO-source in the atmosphere simulation chamber SAPHIR, *Atmos. Chem. Phys.*, 5, 2189–2201, doi:10.5194/acp-5-2189-2005, 2005.

Sarwar, G., Roselle, S. J., Mathur, R., Appel, W., Dennis, R. L., and Vogel, B.: A comparison of CMAQ HONO predictions with observations from the Northeast Oxidant and Particle Study, *Atmos. Environ.*, 42, 5760–5770, 2008.

Stemmler, K., Ammann, M., Donders, C., Kleffmann, J., and George, C.: Photosensitized reduction of nitrogen dioxide on humic acid as a source of nitrous acid, *Nature*, 440, 195–198, 2006.

Stemmler, K., Ndour, M., Elshorbany, Y., Kleffmann, J., D'Anna, B., George, C., Bohn, B., and Ammann, M.: Light induced conversion of nitrogen dioxide into nitrous acid on submicron humic acid aerosol, *Atmos. Chem. Phys.*, 7, 4237–4248, doi:10.5194/acp-7-4237-2007, 2007.

Stutz, J., Oh, H.-J., Whitlow, S. I., Anderson, C. H., Dibb, J. E., Flynn, J., Rappenglück, B., and Lefer, B.: Simultaneous DOAS and Mist-Chamber IC measurements of HONO in Houston, TX, *Atmos. Environ.*, 44, 4090–4098, doi:10.1016/j.atmosenv.2009.02.003, 2010.

Su, H., Cheng, Y. F., Shao, M., Gao, D. F., Yu, Z. Y., Zeng, L. M., Slanina, J., Zhang, Y. H., and Wiedensohler, A.: Nitrous acid (HONO) and its daytime sources at a rural site during the 2004 PRIDE-PRD experiment in China, *J. Geophys. Res.*, 113, D14312, doi:10.1029/2007JD009060, 2008.

Wennberg, P. O. and Dabdub, D.: Rethinking Ozone Production, *Science*, 319, 1624–1625, 2008.

Wilczak, J. M., Djalalova, I., McKeen, S., Bianco, L., Bao, J.-W., Grell, G., Peckham, S., Mathur, R., McQueen, J., and Lee, P.: Analysis of regional meteorology and surface ozone during the TexAQS II field program and an evaluation of the NMM-CMAQ and WRF-Chem air quality models, *J. Geophys. Res.*, 114, D00F14, doi:10.1029/2007JD009060, 2009.

Wong, K. W., Oh, H.-J., Lefer, B. L., Rappenglück, B., and Stutz, J.: Vertical profiles of nitrous acid in the nocturnal urban atmosphere of Houston, TX, *Atmos. Chem. Phys.*, 11, 3595–3609, doi:10.5194/acp-11-3595-2011, 2011.

Zhou, X. L., He, Y., Huang, G., Thornberry, T. D., Carroll, M. A., and Bertman, S. B.: Photochemical production of nitrous acid on glass sample manifold surfaces, *Geophys. Res. Lett.*, 29, 1681, doi:10.1029/2002GL015080, 2002.

Zhou, X. L., Gao, H. L., He, Y., Huang, G., Bertman, S. B., Civerolo, K., and Schwab, J.: Nitric acid photolysis on surfaces in low-NO_x environments: significant atmospheric implications, *Geophys. Res. Lett.*, 30, 23, 2217, doi:10.1029/2003GL018620, 2003.

Ziemba, L. D., Dibb, J. E., Griffin, R. J., Anderson, C. H., Whitlow, S. I., Lefer, B. L., Rappenglück, B., and Flynn, J.: Heterogeneous conversion of nitric acid to nitrous acid on the surface of primary organic aerosol in an urban atmosphere, *Atmos. Environ.*, doi:10.1016/j.atmosenv.2008.12.024, 2010.

Modeling nitrous acid and its impact

B. H. Czader et al.

Title Page

Abstract

Introduction

Conclusions

References

Tables

Figures

⏪

⏩

◀

▶

Back

Close

Full Screen / Esc

Printer-friendly Version

Interactive Discussion



**Modeling nitrous acid
and its impact**

B. H. Czader et al.

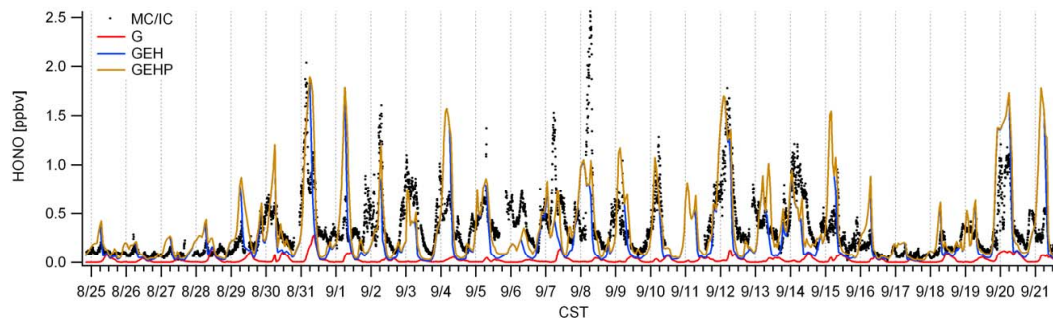


Fig. 1. Comparison of measured vs. simulated HONO time series at the UH Moody Tower for the time period 25 August–21 September 2006. Dots represent measured values obtained in-situ by a MC/IC system, the solid lines represent CMAQ predicted concentration from G, GEH, and GEHP cases (explanation see text). Dashed vertical lines indicate midnight times.

[Title Page](#)[Abstract](#)[Introduction](#)[Conclusions](#)[References](#)[Tables](#)[Figures](#)[◀](#)[▶](#)[◀](#)[▶](#)[Back](#)[Close](#)[Full Screen / Esc](#)[Printer-friendly Version](#)[Interactive Discussion](#)

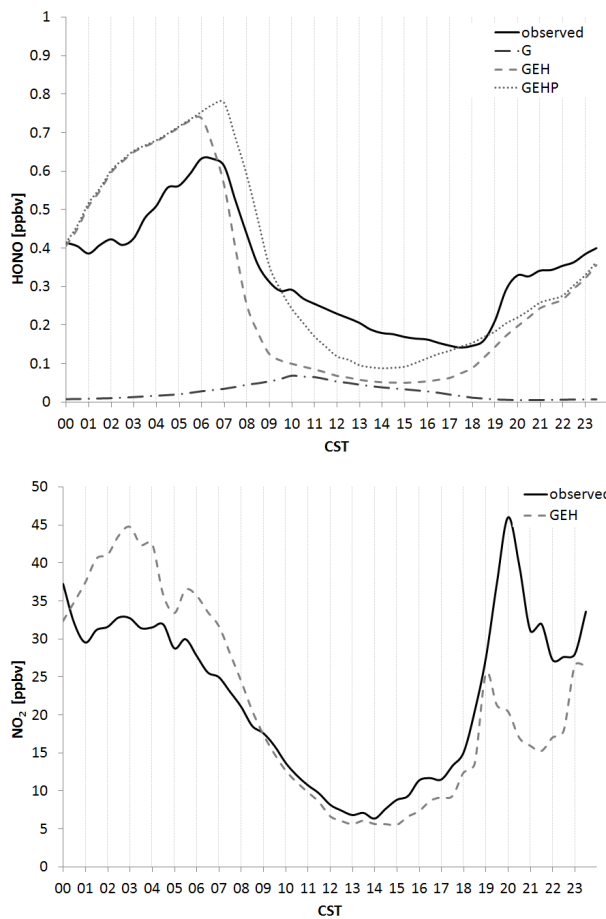


Fig. 2. Average diurnal variation of HONO (top) and NO_2 (bottom) based on data for 25 August–21 September 2006.

Modeling nitrous acid and its impact

B. H. Czader et al.

Title Page

Abstract Introduction

Conclusions References

Tables Figures

◀ ▶

◀ ▶

Back Close

Full Screen / Esc

Printer-friendly Version

Interactive Discussion



Modeling nitrous acid
and its impact

B. H. Czader et al.

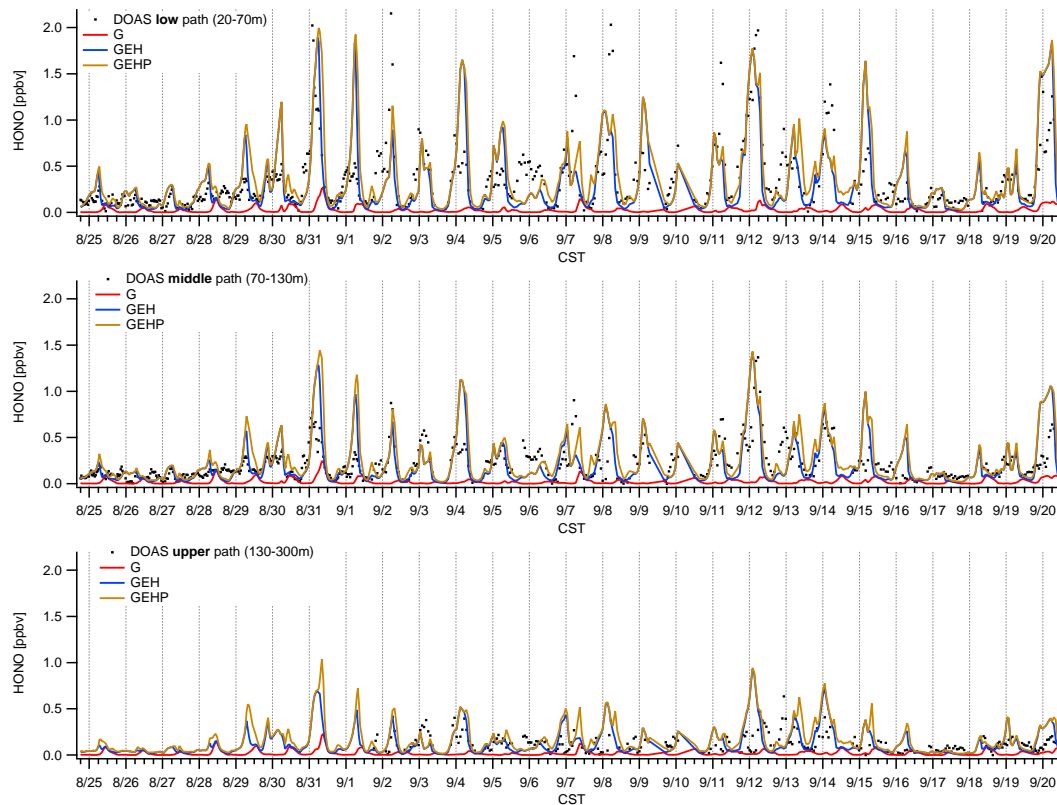


Fig. 3. Time series comparison of HONO measured from the Moody Tower by DOAS low light-path (top graph), middle light path (middle graph), and upper path (bottom graph) with simulated mixing ratios for 25 August–20 September 2006.

[Title Page](#)[Abstract](#)[Introduction](#)[Conclusions](#)[References](#)[Tables](#)[Figures](#)[◀](#)[▶](#)[◀](#)[▶](#)[Back](#)[Close](#)[Full Screen / Esc](#)[Printer-friendly Version](#)[Interactive Discussion](#)

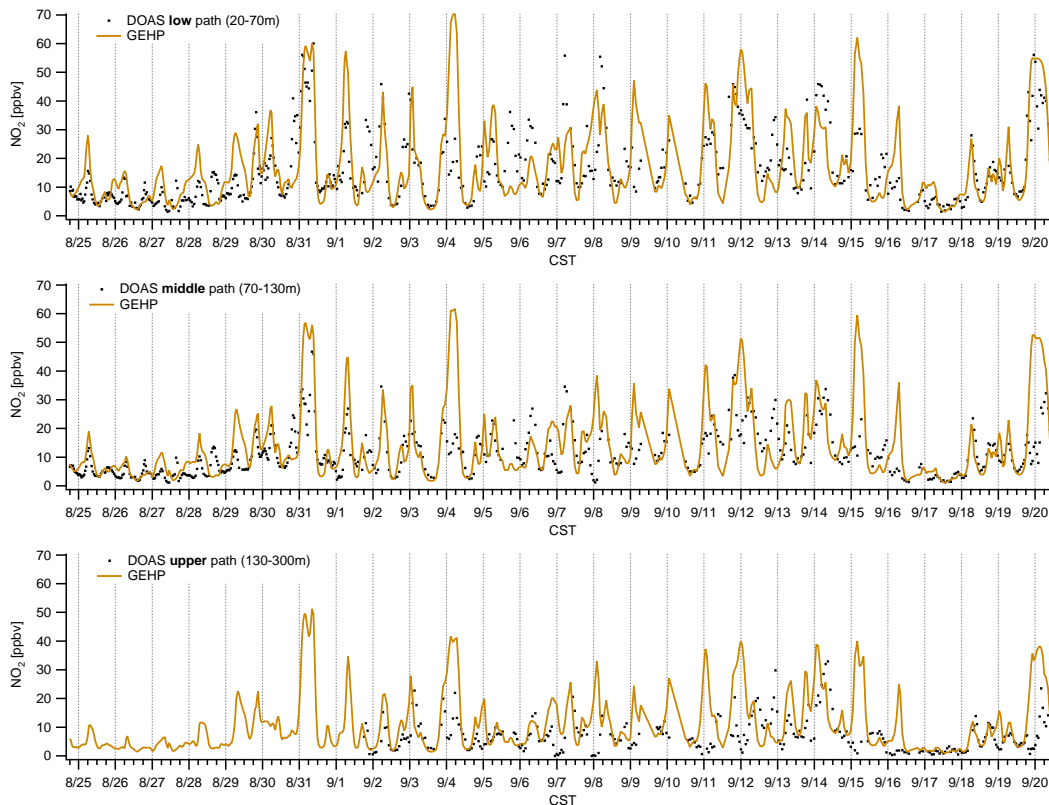


Fig. 4. Time series comparison of NO_2 measured from the Moody Tower by DOAS low light-path (top graph), middle light path (middle graph), and upper path (bottom graph) with simulated mixing ratios for 25 August–20 September 2006.

Modeling nitrous acid and its impact

B. H. Czader et al.

Title Page	
Abstract	Introduction
Conclusions	References
Tables	Figures
◀	▶
◀	▶
Back	Close
Full Screen / Esc	
Printer-friendly Version	
Interactive Discussion	



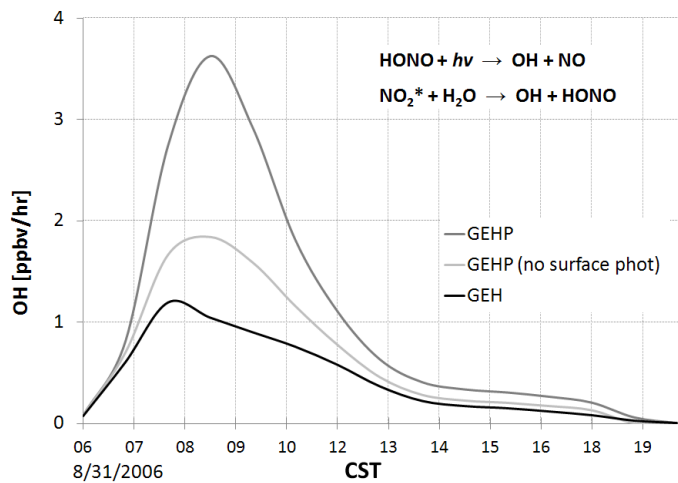
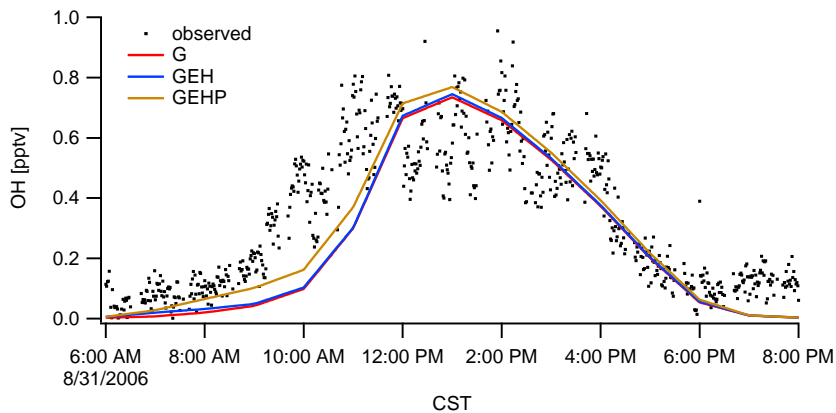


Fig. 5. Top: time series of observed and simulated OH mixing ratios. Bottom: OH production from the reaction of $\text{HONO} + h\nu \rightarrow \text{OH} + \text{NO}$ and $\text{NO}_2^* + \text{H}_2\text{O} \rightarrow \text{OH} + \text{HONO}$.

Modeling nitrous acid and its impact

B. H. Czader et al.

Title Page

Abstract Introduction

Conclusions References

Tables Figures

◀ ▶

◀ ▶

Back Close

Full Screen / Esc

Printer-friendly Version

Interactive Discussion



Modeling nitrous acid and its impact

B. H. Czader et al.

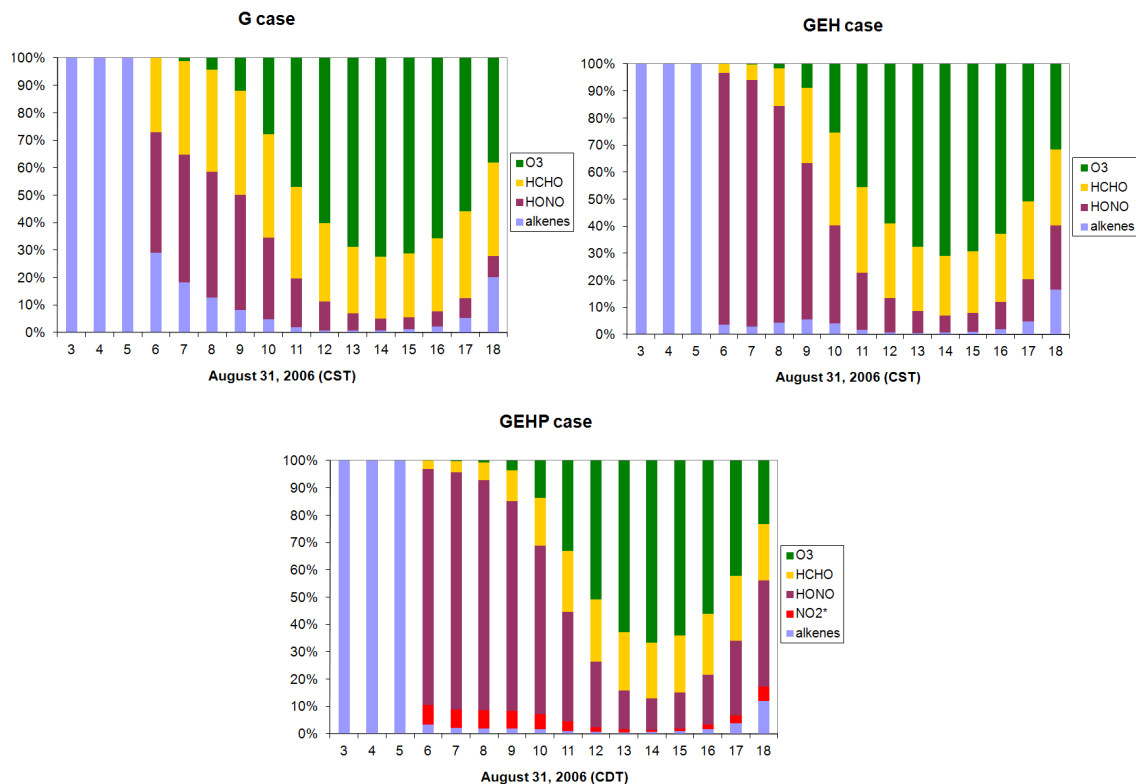


Fig. 6. Diurnal variations of contributions of O₃, HCHO, HONO (from photolysis reaction), NO₂^{*}, and alkenes to the HO_x budget for the G case (top), GEH case (middle), and GEHP case (bottom).

Title Page

Abstract

Introduction

Conclusions

References

Tables

Figures

⏪

⏩

◀

▶

Back

Close

Full Screen / Esc

Printer-friendly Version

Interactive Discussion



Modeling nitrous acid and its impact

B. H. Czader et al.

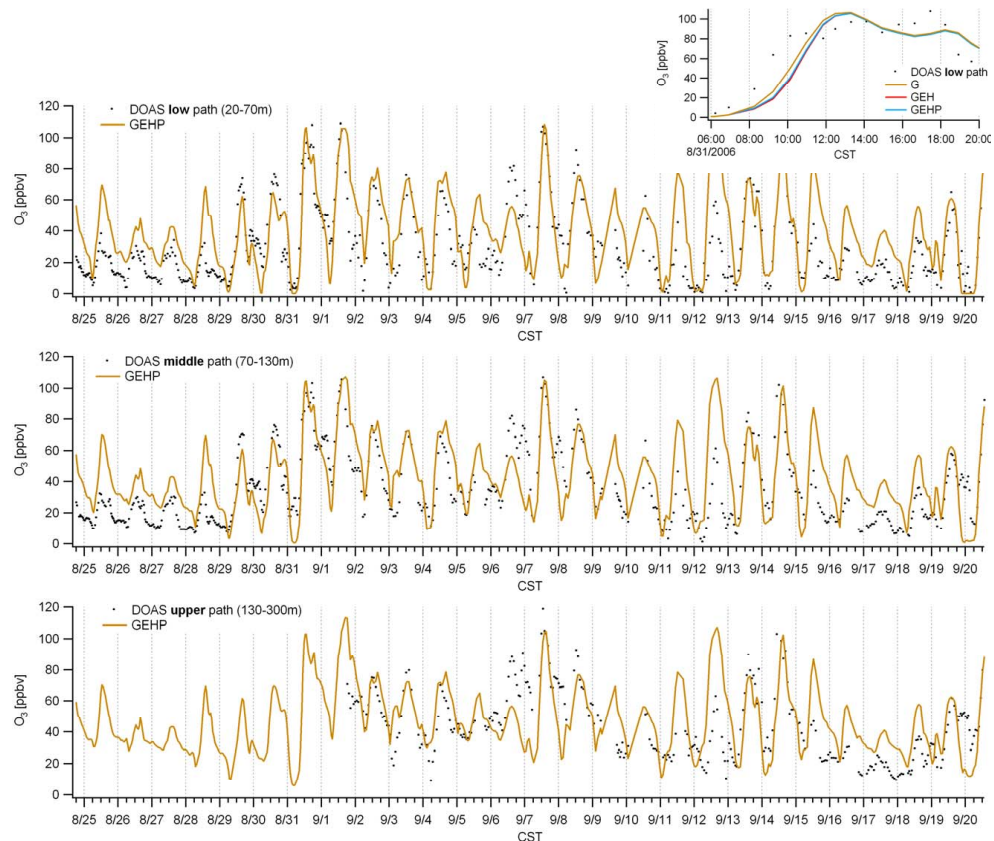


Fig. 7. Time series comparison of O_3 measured from the Moody Tower by DOAS low light-path (top graph), middle light path (middle graph), and upper path (bottom graph) with simulated mixing ratios for 25 August–20 September 2006. The insert shows a blow-up for 31 August 2006, displaying all the three model simulations vs. the observed O_3 data on that day.

Title Page

Abstract

Introduction

Conclusions

References

Tables

Figures

◀

▶

◀

▶

Back

Close

Full Screen / Esc

Printer-friendly Version

Interactive Discussion



Modeling nitrous acid and its impact

B. H. Czader et al.

Title Page

Abstract

Introduction

Conclusions

References

Tables

Figures

◀

▶

◀

▶

Back

Close

Full Screen / Esc

Printer-friendly Version

Interactive Discussion

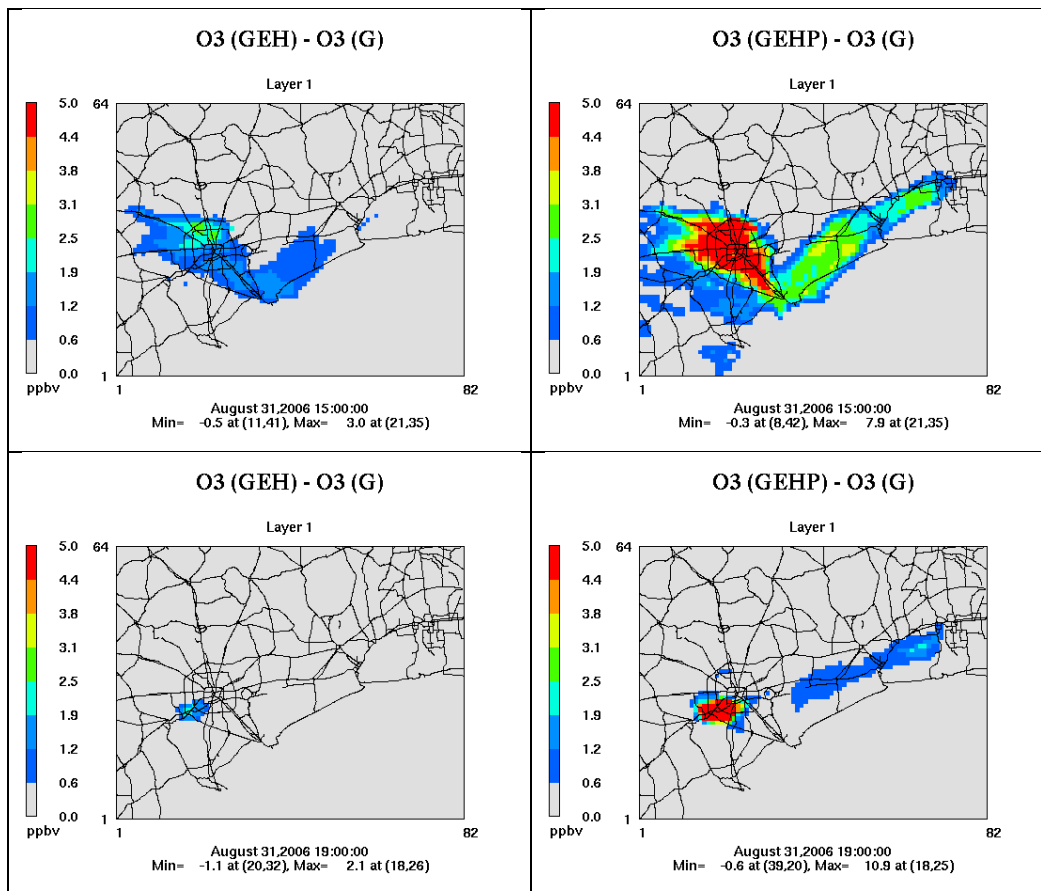


Fig. 8. Differences in ozone simulations between GEH-G case (left) and GEHP-G case (right) for 31 August, 2006 at 00:09 a.m. CST (top) and 01:00 p.m. CST (bottom).

Modeling nitrous acid and its impact

B. H. Czader et al.

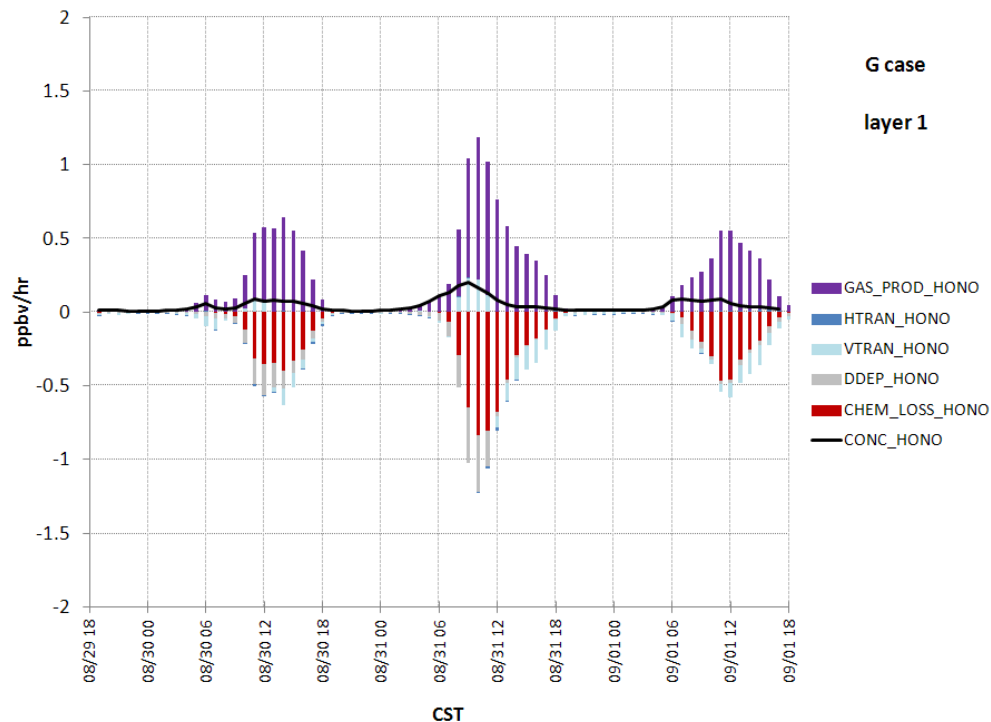


Fig. 9. HONO mixing ratio (black line) in ppbv and contribution of different processes to changes in HONO mixing ratios (columns) in ppbv h^{-1} for G case (top), GEH case (middle), and GEHP case (bottom) in the first model layer. Note that the scale is different in the graphs. GAS_PROD_HONO represents OH+NO reaction producing HONO, $\text{hv_NO}_2^*_\text{HONO}$ is HONO formed from excited NO_2 , hv_SF_HONO – is photochemical production of HONO on surfaces, HET_HONO represents change in HONO mixing ratio due to heterogeneous chemistry, VTRAN_HONO – vertical transport, HTRAN_HONO – horizontal transport, DDEP_HONO – dry deposition, CHEM_LOSS_HONO – loss of HONO by gas phase chemical reactions, EMIS_HONO – emissions.

Title Page

Abstract

Introduction

Conclusions

References

Tables

Figures

◀

▶

◀

▶

Back

Close

Full Screen / Esc

Printer-friendly Version

Interactive Discussion



**Modeling nitrous acid
and its impact**

B. H. Czader et al.

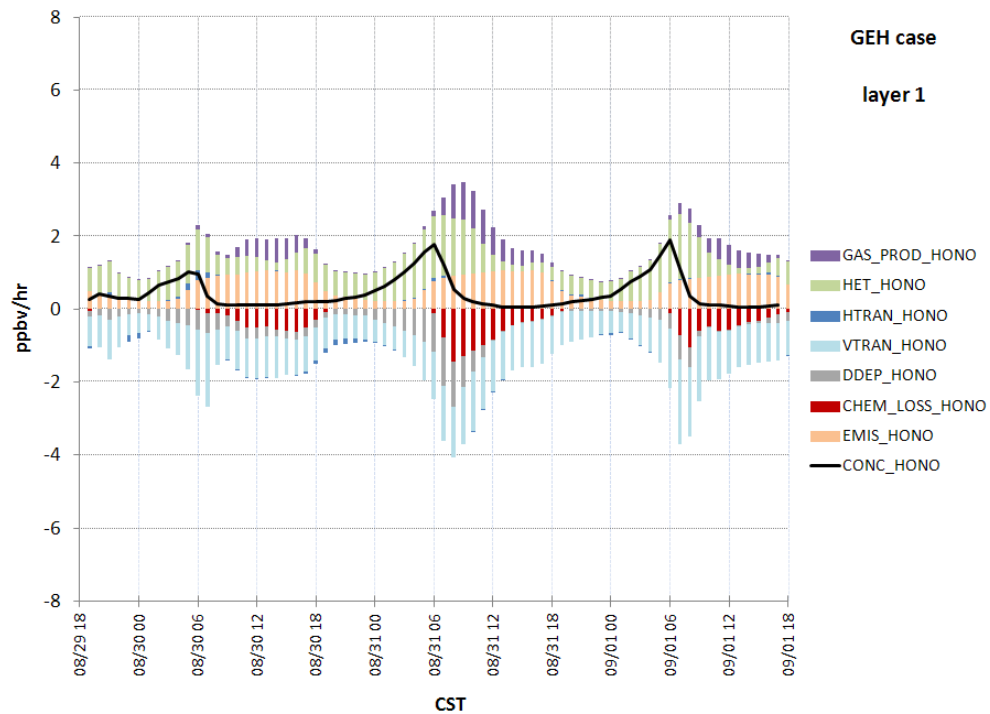


Fig. 9. Continued.

[Title Page](#)[Abstract](#)[Introduction](#)[Conclusions](#)[References](#)[Tables](#)[Figures](#)[◀](#)[▶](#)[◀](#)[▶](#)[Back](#)[Close](#)[Full Screen / Esc](#)[Printer-friendly Version](#)[Interactive Discussion](#)

**Modeling nitrous acid
and its impact**

B. H. Czader et al.

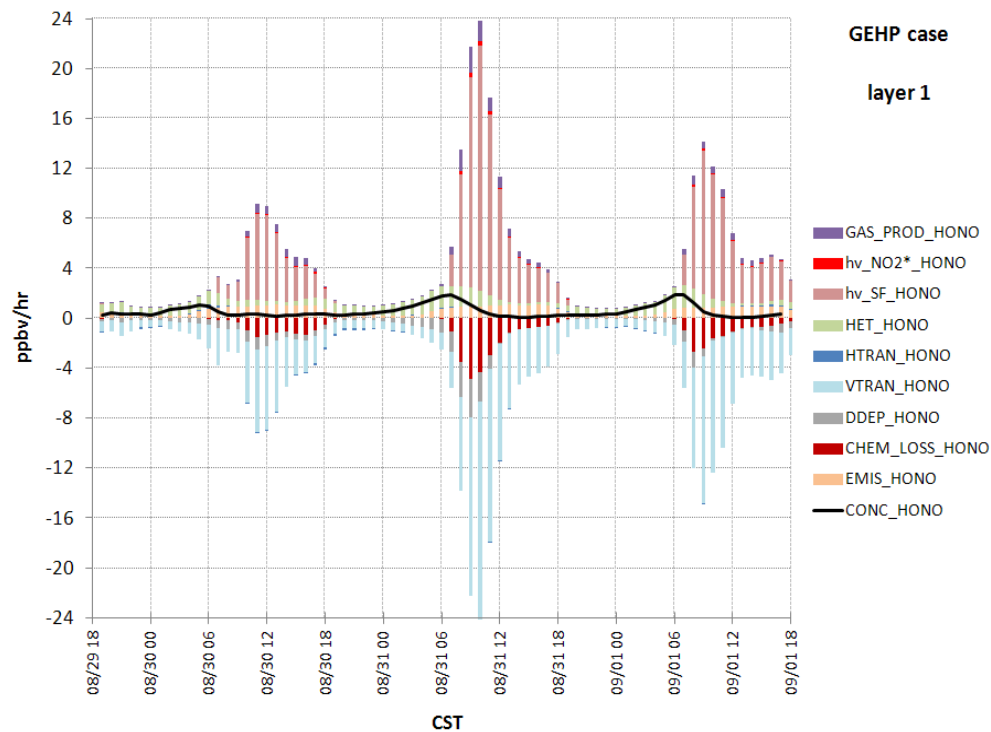


Fig. 9. Continued.

[Title Page](#)[Abstract](#)[Introduction](#)[Conclusions](#)[References](#)[Tables](#)[Figures](#)[◀](#)[▶](#)[◀](#)[▶](#)[Back](#)[Close](#)[Full Screen / Esc](#)[Printer-friendly Version](#)[Interactive Discussion](#)